

Ionization and ionization–excitation of helium to the $n=1-4$ states of He^+ by electron impactS. Bellm,¹ J. Lower,² K. Bartschat,³ X. Guan,³ D. Weflen,³ M. Foster,⁴ A. L. Harris,⁵ and D. H. Madison⁵¹*AMPL, Research School of Physical Sciences and Engineering, Australian National University, Canberra, ACT 0200, Australia*²*Centre for Antimatter-Matter Studies, Australian National University, Canberra, ACT 0200, Australia*³*Department of Physics and Astronomy, Drake University, Des Moines, Iowa 50311, USA*⁴*Theoretical Division T-4 B-283, Los Alamos National Laboratory, Los Alamos, New Mexico 87545, USA*⁵*University of Missouri-Rolla, 1870 Miner Circle, Rolla, Missouri 65409, USA*

(Received 17 December 2006; revised manuscript received 23 January 2007; published 11 April 2007)

We present experimental and theoretical results for the electron-impact-induced ionization of ground-state helium atoms. Using a high-sensitivity toroidal electron spectrometer, we measured cross-section ratios for transitions leading to the first three excited states of the residual helium ion relative to the transition leaving the ion in the ground state. Measurements were performed for both symmetric- and asymmetric-energy-sharing kinematics. By presenting results as a ratio, a direct comparison can be made between theoretical and experimental predictions without recourse to normalization. The experimental data are compared to theoretical predictions employing various first-order models and a second-order hybrid distorted-wave + convergent R matrix with pseudostates (close-coupling) approach. All the first-order models fail in predicting even the approximate size of the cross-section ratios. The second-order calculations are found to describe the experimental data for asymmetric-energy-sharing with reasonable fidelity, although significant disparities are evident for the symmetric-energy-sharing cases. These comparisons demonstrate the need for further theoretical developments, in which all four charged particles are treated on an equal footing.

DOI: [10.1103/PhysRevA.75.042704](https://doi.org/10.1103/PhysRevA.75.042704)

PACS number(s): 34.80.Dp, 34.80.Pa

I. INTRODUCTION

Studies of electron-impact-induced ionization are of interest from both theoretical and practical perspectives. In the former case, ionizing collisions of electrons with isolated atoms and molecules provide insight into the many-body behavior of bound states and mechanisms driving fragmentation processes, facilitating the development of sophisticated theoretical approaches. In the latter, accurate modeling of complex systems such as gas discharges, lasers, and the physics and chemistry of the upper atmosphere depends on the provision of accurate ionization cross sections, their predictive powers limited by the quality of the cross-section data, which they incorporate.

In recent years there have been dramatic improvements in both experimental and theoretical or computational methods for treating the ionization problem. On the experimental front, multiparameter time-of-flight detection systems such as COLTRIMS (cold atom recoil ion momentum spectroscopy) [1] or the “reaction microscope” [2] have enabled large volumes of momentum phase space (defined by the momenta of the ionization fragments) to be collected in parallel and provided access to regions of momentum phase space inaccessible to conventional spectrometers. Furthermore, ionization experiments of unparalleled complexity are now possible due to multihit detection systems, which allow multiple charged particles arising from single- or multiple-ionization atomic- or molecular-fragmentation-events to be recorded, preserving the momentum correlation between all fragments [3]. As a result, an entire new area of ionization experiments has been opened up.

Concurrently, momentum-dispersive spectrometers based around electrodes of toroidal geometry have successfully demonstrated their capacity to collect data over smaller re-

gions of phase space with high precision, because of their abilities to operate with a continuous projectile beam and their intrinsically high momentum resolution at moderate to high electron energies [4–8].

In parallel to these developments, theory has now reached a sufficient degree of sophistication to computationally solve the ionization of atomic hydrogen by electron impact (the Coulomb three-body problem) to an arbitrary degree of accuracy. Nonperturbative approaches such as exterior complex scaling (ECS) [9], time-dependent close-coupling (TDCC) [10], convergent close coupling (CCC) [11], or R matrix with pseudostates (RMPS) [12] are now able to predict the total (TCS), single-differential (SDCS), double-differential (DDCS), and triple-differential (TDCS) cross section very accurately for this system, with the accuracy limit essentially set by the available computational resources and the algorithm stability.

In contrast, the solution of the Coulomb four-body problem still remains a considerable theoretical and computational challenge. For cases in which one of the four electrons essentially acts as a spectator (e.g., ionization without simultaneous excitation of the residual ion), agreement with convergent close-coupling calculations is generally very good for electron-impact-induced ionization and electron emissions in and out of the scattering plane [13–16]). Good agreement for this case is perhaps not so surprising, as the overlap of the He^+1s orbital with the Hartree-Fock $1s$ of helium is still close to unity, i.e., the remaining bound electron does not change its quantum state significantly. Hence, the four-body problem effectively reduces to one with largely three-body character. Even for such quasi three-body cases, however, recent work [16] on helium has shown the importance of accurately describing higher-order scattering effects when treating out-of-plane scattering geometries. Higher-order, as well as correlation effects, are also critical

in true four-body Coulomb problems such as ionization plus simultaneous excitation or double ionization. Significant discrepancies exist between experimental data and predictions from various second-order theories [17–22] or so-called “3C” [23–25] and “3DW” [26–30] versions, which account for the correct asymptotic Coulomb boundary-condition.

For scattering of highly charged nuclei from the helium atom, significant discrepancies also remain between experiment and the best calculations presently available, as demonstrated by Schulz *et al.* [31] for 100 MeV/amu C^{6+} heavy-particle impact ionization of helium. An important step towards resolving this problem appears to have been made by Foster *et al.* [32], who recently examined the effects of different theoretical approximations in describing the electron-impact-induced ionization of magnesium. In that work, distorted-wave calculations, which describe the radially-dependent effective-charge determined by the electron-cloud screening of the nucleus, were able to reproduce out-of-plane cross sections, while 3DW calculations, for which the effective charge seen by the projectile is unity at all distances from the ion, could not. Given that the 3DW approach was also employed in Ref. [31], the authors concluded that the failure of the theoretical models for out-of-plane heavy-particle scattering might be due to a poor representation of the heavy-projectile wave function at small impact parameters. It therefore appears that an accurate treatment of the screening of the helium nuclear potential by the remaining bound electron may be crucial to describe high-momentum transfer (low impact-parameter) ion-helium collisions.

In contrast to the electron-helium and ion-helium scattering cases considered above, for the ionization–excitation process considered in this work, *both* target electrons undergo significant changes in their quantum states, thereby providing a severe challenge to theory. Even for the coplanar geometry, significant discrepancies between theory and experiment can occur under such conditions, if the part of the projectile-target interaction responsible for ionization is only accounted for to first order [33]. To date, ($e, 2e$) experimental data for this process have been somewhat sparse. This is primarily due to the small cross sections involved, with the fraction of single-ionization events involving excitation of the residual ion only accounting for around 1% of those leaving the ion in its ground state. Furthermore, if one wishes to measure the higher lying ionic states $n > 2$, good energy resolution is required as the excitation limits converge to the double-ionization limit with increasing values of n . This further exacerbates the problem, as obtaining good experimental energy resolution is usually at the expense of instrumental collection efficiency.

Early experimental work on the helium ionization–excitation problem was performed in coplanar [34] or noncoplanar [35,36] scattering geometries under electron momentum spectroscopy (EMS) conditions of high impact-energies and high-momentum-transfer symmetric-energy-sharing collisions. From these experiments electron momentum distributions for the $n=2$ and $n=3$ states of the residual ion were derived by assuming the validity of the impulse approximation. These results were used as a basis to compare different theoretical descriptions of the correlated helium ground-state wave function.

Subsequent experiments were carried out under asymmetric-scattering conditions in which the energy of the measured scattered-projectile electron was much higher than that of the ejected electron, which was typically detected at considerably lower energies. When a low-energy continuum electron is involved, the theoretical description is much more difficult than for the high-energy kinematics of EMS experiments. Stefani *et al.* [37] measured transitions to the $n=2$ ion states at an incident beam energy of 1585 eV, a scattering angle of 4° for the fast scattered projectile (1500 eV), and an ejected-electron energy of 20 eV. Subsequently, Dupré *et al.* [38] reported measurements at an incident beam energy of 5.5 keV for ejected-electron energies of 5, 10, and 75 eV. Avaldi *et al.* [39] performed measurements at incident-beam energies of ≈ 1600 and 600 eV, respectively, and ejected-electron energies of 10, 20, and 40 eV. Asymmetric measurements were also performed by Rouvellou *et al.* [40] for 366 eV incident electrons and an ejected-electron energy of 9 eV. All of these experiments involved a highly-asymmetric energy-sharing between the two continuum electrons. For such cases, hybrid methods based upon a perturbative treatment, up to second order, of the projectile-target interaction and an R -matrix (close-coupling) approach for the ejected-electron–residual-ion interaction [41] have been quite successful, especially when the latter part of the problem (e -He $^+$ collisions) was systematically driven to convergence [19]. Except for Dogan and Crowe [42], and our previously reported experiment [17], which is expanded upon in this paper, all previous asymmetric-energy-sharing TDCS experiments have been restricted to ionization–excitation to the $n=2$ residual ionic states. In Ref. [42], measurements were performed at an electron-impact energy of 200 eV and ($e, 2e$) angular correlations for the $n=2$ to $n=4$ excited states presented. More recently, under high-energy symmetric non-coplanar geometry, ionization–excitation measurements were performed at energies of 2080 eV [43] and at 1000 and 1600 eV [44], respectively, using advanced multiparameter spectrometers. In the former case, ionization–excitation leading to the $n=1$ and $n=2$ ion states was considered and first-order plane-wave impulse approximation (PWIA) calculations were used to assess the quality of various target wave functions. In the latter case, the impact-energy dependence of the cross-section ratios for the He $^+$ $n=1, 2$, and 3 final ion states was measured.

Because of the energy degeneracy of the He $^+(2s)$ and He $^+(2p)$ states, for all of the experiments described above the measured TDCS was the sum of their respective contributions. Sakhelashvili *et al.* [45], however, by also detecting the emitted $2p \rightarrow 2s$ photon in a triple-coincidence ($e, \gamma 2e$) measurement, were able to derive angular correlations for transitions to the $2p$ ionic states. Comparing their experimental results with state-of-the-art numerical calculations, they found that a first-order treatment of the projectile-target interaction can reproduce the *relative* angular dependence of the experimental data at large momentum transfers. However, consistent magnitudes between the cross-normalized experimental data could only be obtained in a second-order treatment.

Further challenges to four-body collision theory arise when, in addition to three electrons each changing their

quantum state significantly, the incident- and final-state electrons all have low energies. Using a noncoplanar-symmetric scattering-geometry, Murray and Read [46] performed measurements at 145 eV incident energy for scattered electron energies of 45 eV. To our knowledge, no calculations to model these results have yet been published, thereby indicating the difficulty of the task.

In our earlier publication [17], we presented a comparison of measured and calculated cross-section ratios for ionization and excitation of the first three excited states of He^+ relative to the ground state at incident energies between 112 and 319 eV for selected kinematics. Here, we present a much more extensive body of experimental and theoretical results, this time comparing predictions from a number of different theoretical approaches. The motivation for the experiment was already briefly described in Ref. [17]. The principal purpose is to provide a benchmark data set to compare state-of-the-art scattering theories, avoiding problems associated with comparisons of previous experimental and theoretical data. In particular, all previous asymmetric-energy-sharing experimental TDCS studies of ionization–excitation of helium suffered from at least one of the following drawbacks.

First, all of the measured data were relative and had to be normalized to theory or other absolute experimental data for comparison. In the present case, the data are presented as a high-accuracy *ratio* of cross sections for excitation of the $n \geq 2$ ionic states relative to the $n=1$ “transition with a spectator” ionic state. This allows results to be directly compared to theory without the need for normalization, thereby avoiding errors attendant to this procedure.

Second, poor statistical accuracy characterized many previous experiments. This could be traced back to their use of single-parameter data-collection techniques, where points in momentum phase-space are sequentially scanned in energy and/or scattering angle for the two ejected electrons. For the present study, as in Ref. [45], more sophisticated multiparameter techniques have been employed. These allow for the measurement to be performed over a larger volume of momentum phase space while maintaining good energy resolution.

Third, with the exception of one study [42], previous asymmetric measurements did not extend to ionization of the $n > 2$ excited states. This was presumably due to the trade-off in count rate that would have been required to achieve the energy resolution needed to resolve the higher-lying ion states as they converge to the double ionization limit. Furthermore, as the value of n increases, cross sections rapidly decrease, thereby further lengthening the time required to acquire data of a given statistical accuracy. By measuring excitation cross sections to these higher-lying states in the present work, we provide an even more stringent test to theory of the four-body electron-atom collision problem and new impetus for further developments.

Finally, in many of the previous experiments the energy of one of the two final-state continuum electrons was chosen in the energy range between 5 and 10 eV. This range is problematic for theory, as it is associated with the $n=3$ and $n=4$ doubly-excited resonance-states of helium, making a straightforward comparison with theoretical predictions almost impossible [47] if the theory treats the $e\text{-He}^+$ problem

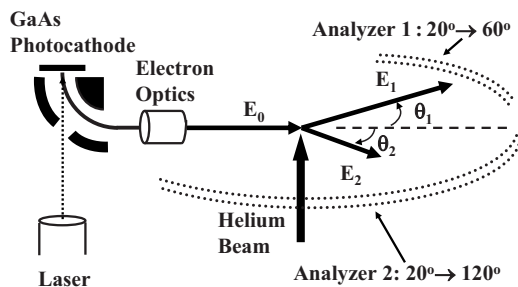


FIG. 1. Scheme of the apparatus. See the text for details.

via the generally desirable close-coupling approach.

In summary, the present experimental work is an attempt to build upon the strengths of previous studies and, where possible, to improve upon some of their deficiencies. To this end, we have applied our high-efficiency multiparameter toroidal spectrometer [4] to the problem, which enables us to achieve high data rates while still achieving sufficient energy resolution to resolve $n > 2$ states.

II. APPARATUS AND EXPERIMENTAL TECHNIQUES

Figure 1 shows a schematic representation of the present experimental apparatus. A short description will be given here, with further details to be found in Ref. [48]. A primary beam of electrons is created by illuminating a strained gallium arsenide photocathode by monochromatic 850 nm laser light under ultrahigh-vacuum conditions in our so-called source chamber. The cathode is similar in structure to that employed by Nakanishi *et al.* [49] and is used by our group to produce polarized electrons when illuminated by circularly polarized light. In the present experiment, where no spin-dependent effects were anticipated, measurements were performed with an ensemble of unpolarized electrons formed by illuminating the photocathode sequentially by right- and left-circularly-polarized light for equal measurement times. After extraction by a weak electrostatic field, the beam is deflected through 90° before being accelerated to 600 eV for transport through a differentially-pumped chamber (the differential chamber) before entering the collision chamber, where it is decelerated to the experimental collision-energy E_0 and focused on to the helium target beam. The purpose of initially accelerating the beam is to reduce its spatial profile in transport from the source chamber to the collision chamber. This enables it to be guided through small apertures, allowing the ambient pressure at the GaAs photocathode to be maintained at low values when target gas is introduced to the collision chamber. A five-element cylindrical electrostatic lens is used to focus the electron beam on to the helium beam at right angles, their overlap defining a localized interaction volume. The helium target beam is formed by effusion through a 1-mm-internal-diameter molybdenum needle with the electron beam passing 1 mm above its orifice.

The final-state ($e, 2e$) electrons are momentum analyzed using two toroidal-sector electrostatic energy analyzers. Coplanar scattering geometry is employed, meaning that only ($e, 2e$) electron pairs emitted within a plane containing the primary-electron beam are detected. Each analyzer incorpo-

rates a pair of (microchannel-plate) electron-multipliers followed by a crossed-delay-line detector. This detector determines the spatial and temporal electron-arrival coordinates (x_i, y_i, t_i) [1]. From these coordinates, pairs of electrons derived from common ($e, 2e$) ionization events are identified by their correlated arrival times at the two separate detectors, and their initial momenta $(\mathbf{p}_1, \mathbf{p}_2)$ are deduced. One analyzer accepts electrons over the angular range $20^\circ \leq \theta_1 \leq 60^\circ$, while the other accepts electrons over the range $20^\circ \leq \theta_2 \leq 120^\circ$. Due to the limited size of the detectors (80 mm diameter) only a 40° band of emission angles can be measured in each analyzer. For the smaller analyzer the detector is fixed, to encompass the angular range $20^\circ \leq \theta_1 \leq 60^\circ$. For the larger analyzer the detector is movable, enabling the mean angle of the detection range to be varied from 40° to 100° . For the present experiment, successive measurements were performed at three positions for this detector to enable access to the full range of emission angles $20^\circ \leq \theta_2 \leq 120^\circ$.

Two experiments were performed, one for symmetric- and one for asymmetric-energy-sharing between the final-state continuum-electron pairs. The average scattered- or ejected-electron energies E_1 and E_2 were 200 and 44 eV, respectively, for the asymmetric-energy-sharing case and 44 and 44 eV for the symmetric case. From energy conservation, the corresponding values for the collision energy E_0 for ionization leading to the $\text{He}^+(1s)$ ground state were 268.6 and 112.6 eV for the asymmetric and symmetric cases, respectively. In the asymmetric case, the slow-electron energy band was strategically chosen in a region absent of resonance contributions, and sufficiently high in energy that we could accurately energy-calibrate our analyzers by elastic scattering measurements (our present electron gun only operates effectively above 35 eV). The fast ejected-electron energy was then chosen sufficiently high to justify use of a perturbative treatment of the “fast” ejected-electron, but low enough to ensure sufficiently high count rates to make measurement of the $n \geq 2$ higher-excited ion states feasible. For the symmetric experiment, the common value of 44 eV was selected for the ejected electrons to facilitate an assessment of how approximations used in the treatment of the “fast” scattered electron break down as the incident-beam energy is lowered.

To maintain the same average scattered or ejected electron energies for ionization–excitation as for ionization leading to the $\text{He}^+(1s)$ ground state, the value of the incident beam energy should be increased by 40.8 eV ($n=2$), 48.4 eV ($n=3$), and 51.0 eV ($n=4$). However, to reduce the data collection time for the symmetric-energy-sharing experiment, the primary-electron beam energy was maintained at the $n=3$ value of 161.0 eV when performing the $n=4$ measurement, resulting in a reduced average energy of 42.7 eV for the two final-state electrons in that case. This 1.3 eV difference was not taken into account for the $n=4$ calculations. However, due to its small magnitude it was not expected to profoundly affect the comparison of theory and experiment. For the asymmetric experiment, coincident events were accepted over a 16 eV energy window in each analyzer, i.e., $192 \text{ eV} \leq E_1 \leq 208 \text{ eV}$, $36 \text{ eV} \leq E_2 \leq 52 \text{ eV}$ while providing sufficient energy resolution to resolve the first two excited states. For the weak ionization–excitation processes consid-

ered in this work, operating our spectrometer with a large energy-acceptance window was a necessary trade-off to obtain data of adequate statistical accuracy. Nevertheless, using the experience we gained through this experiment, improvements in techniques were wrought, enabling us to reduce the analyzer acceptance-energy windows for the symmetric case to 8 eV, i.e., $40 \text{ eV} \leq E_1 \leq 48 \text{ eV}$, $40 \text{ eV} \leq E_2 \leq 48 \text{ eV}$ while still maintaining good counting statistics. The improved resolution achieved by operating with a smaller energy-acceptance band enabled us to additionally resolve $n=4$ contributions in that case. Within each window, electron energies were determined to within 0.65 eV (asymmetric kinematics) and 0.40 eV (symmetric kinematics). Combined with an energy spread of 0.30 eV for the primary beam, values of 1.0 and 0.65 eV binding energy resolution were, respectively, achieved for the asymmetric and symmetric experiments. To ensure an accurate cross normalization, the beam-focusing optics was adjusted as the incident energy was changed. This was undertaken to minimize energy-dependent changes in the electron-beam profile and hence changes to the interaction-volume geometry. Additionally, the beam current was recorded at each incident energy in a Faraday cup positioned behind the interaction region to enable energy-dependent changes in current to be corrected for in software. For both experiments, E_0 was stepped to ensure each excited-ion-state transition was measured with the same average scattered or ejected-electron energies and for an equal collection time. This process was repeated many times an hour to average over any long-term instrumental drifts and ensure equal collection time for each measured ($e, 2e$) electron pair.

III. THEORETICAL TREATMENTS

In this section we first present an historical overview of the processes of interest, followed by a discussion of the two approaches used in the current work. In the first part, first-order treatments are applied to assess the sensitivity of the results to the description of the initial bound state. In the second, a hybrid model, treating the projectile-target interaction in first- and second-order, is used to assess the importance of higher-order and nonperturbative treatments.

A. History of developments

As mentioned above, an accurate numerical treatment of simultaneous ionization–excitation by electron impact has provided a major challenge to atomic collision theory. Already at the global level of angle-integrated cross sections, a major controversy exists regarding the absolute value of the *total* cross section for simultaneous ionization plus excitation of helium, specifically for leaving the He^+ ion in the excited $(2p)^2P$ state. While the incident-energy dependence of this cross section, integrated over all detection angles of, and energy sharings between, the two outgoing electrons, agrees well in various experimental studies, putting the experimental numbers on the absolute scale turned out to be a major challenge. There are many reasons for the experimental difficulties, including low analyzer efficiencies, relatively small signals compared to competing processes, and the need for

several cross normalizations to other processes for which the cross sections are better known, or to theoretical results. Detailed discussions of these aspects can be found in the experimental papers by Dogan *et al.* [50] or Merabet *et al.* [51].

Recently, Vorov and Bartschat [52] analyzed the theoretical problem further and traced the discrepancies among various first-order perturbative results back to a single matrix element, which turned out to be highly sensitive to the details of the numerical model. To our knowledge, the only fully nonperturbative calculation for the above process was performed by Pindzola *et al.* [53], who solved the time-dependent Schrödinger equation for all three electrons and extracted the results without relying on explicit boundary conditions in the final state. No independent check of the TDCC results are currently available, since the difficulties associated with a third active electron have so far prevented the application of other approaches, such as R matrix with pseudostates (RMPS) [54,55], convergent close-coupling (CCC) [56,57], or exterior complex scaling (ECS) [9,58] to this problem. Also, the TDCC has not yet been applied to TDCS calculations, due to the very large computational resources required [59].

Moving on to angle-differential cross sections, an early calculation based on a perturbative method was performed by McCarthy *et al.* [34], with the principal goal of achieving information about the quality of the wave function for the initial $\text{He}(1s^2)$ bound state. For the symmetric-energy-sharing case and an incident-projectile energy of just above 800 eV, they found that the ionization–excitation process could only be described in reasonable agreement with experiment if a correlated bound-state wave function rather than a single-configuration Hartree-Fock description was used. Later, Franz and Altick [60] extended the first-order plane-wave theory of the process by accounting for the correlation of the two outgoing electrons through the asymptotically correct behavior of the “3C wave function,” which treats the Coulomb interaction between all three particles (the He^+ ion and the two outgoing electrons) on an equal footing [24]. In a later paper [61], Franz and Altick extended the first-order plane-wave theory of ionization–excitation by approximately including the projectile-target interaction to second order. They found significant effects due to the second-order terms, but could not resolve the above-mentioned controversy about the angle-integrated cross sections. Very recently, Chen and Madison [20] also developed a second-order theory. While they used single-channel orbitals and neglected exchange effects between the continuum electrons and the target, the importance of that work was the possibility to obtain the second-order amplitude in their model to numerical accuracy. They, too, found strong second-order effects, but significant discrepancies between their results and experiment remained. This suggested that other aspects of their calculation, such as the treatment of the ejected-electron–residual-ion interaction and/or the initial bound state, were not sufficiently accurate.

Other theoretical attempts to solve the problem are based on various hybrid models, in which the interaction of the projectile electron with the target is described by a plane-wave or a distorted-wave approach, while the ejected-electron–residual-ion interaction is treated via a close-

coupling ansatz [62,63]. The same approach, or other sophisticated representations, are used for the initial $\text{He}(1s^2)$ bound state. The principal advantage of this approach over fully perturbative methods is the highly-correlated treatment of the near-nucleus region for the ejected-electron–residual-ion interaction, including exchange effects to numerical accuracy and channel coupling possibly to convergence (see below). On the other hand, accounting for the electron-electron correlation in the asymptotic region is a major challenge in this approach and, to our knowledge, has not yet been achieved.

Results for angle-integrated cross sections using these models were obtained by Rudge [64] (plane-wave plus three-state close coupling), Raeker *et al.* [65] (distorted-wave plus six-state close coupling), and Bartschat and Grum-Grzhimailo [66]. The latter results, obtained within a distorted-wave model for the projectile and a convergent R matrix with pseudostates (RMPS) close-coupling treatment of the initial bound state and the ejected-electron–residual-ion interaction, finally established a converged (with respect to the number of coupled states) first-order benchmark. Nevertheless, neither of these calculations could resolve the controversy in the total cross sections. For details, see Refs. [51,52].

A way to account for projectile-target effects in a second-order distorted-wave hybrid approach was described by Reid *et al.* [21], but they only applied it to direct ionization of helium with the residual ion left in the $\text{He}^+(1s)$ ground state. Marchalant *et al.* [41] developed a second-order plane-wave hybrid approach and achieved reasonable agreement with the few existing experimental data sets for ionization–excitation in the asymmetric-energy-sharing case. However, Kheifets *et al.* [67] pointed out that the first-order results of Marchalant *et al.* [41] were not converged with the number of states included in the close-coupling expansion of the (slow) ejected-electron–residual-ion interaction. Using a well-defined hybrid model consisting of a plane-wave description for the projectile and convergent close-coupling or R -matrix with pseudostates expansions for the latter problem, they established first-order benchmark results, which were confirmed by Marchalant *et al.* [68] in a subsequent paper. Also, using either a multiterm Hylleraas or an RMPS description of the initial bound state was apparently sufficient to remove any strong dependence of the results on the representation of the $\text{He}^+(1s^2)$ state.

A convergent second-order plane-wave RMPS hybrid model was presented by Fang and Bartschat [19]. They obtained very satisfactory agreement with experiment and, in addition, noticed [47] that in many cases the comparison with existing datasets was not particularly meaningful, due to the unfortunate choice of ejected-electron energies, especially 5 and 10 eV, which lie in the region encompassing contributions from $n=3$ and $n=4$ doubly excited resonance states of helium. Building on the rapid advances of computational power, Kheifets [69] developed a second-order plane-wave CCC approach, albeit restricting the second-order contributions to only the dipole term in the Coulomb interaction. Finally, a convergent second-order distorted-wave RMPS approach, developed by Bartschat based on the original formulation of Reid *et al.* [21], was very successful

in reproducing the experimental data of Sakhelashvili *et al.* [45]. It also presented a major improvement over the corresponding first-order hybrid model when compared with a small subset of our current experimental data [17].

B. First-order Born approach

To assess the sensitivity of the results to the description of the initial bound state, two first-Born calculations were performed. In these calculations the “fast” electron is treated as a plane wave in both the initial- and final-states, and the “slow” electron is treated using a distorted wave. The T matrix for this model is given by

$$T_{fi} = \langle \beta_f(\mathbf{r}_1) \psi_f^{(-)}(\mathbf{r}_2) \psi_{nlm}(\mathbf{r}_3) | V_i | \beta_i(\mathbf{r}_1) \psi_i(\mathbf{r}_2, \mathbf{r}_3) \rangle, \quad (1)$$

with

$$V_i = -\frac{2}{r_1} + \frac{1}{|\mathbf{r}_1 - \mathbf{r}_2|} + \frac{1}{|\mathbf{r}_1 - \mathbf{r}_3|}, \quad (2)$$

where \mathbf{r}_1 is the projectile coordinate while \mathbf{r}_2 and \mathbf{r}_3 are the coordinates of the atomic electrons. Here, $\beta_{i,f}(\mathbf{r}_1)$ is the plane wave representing the “fast” electron, $\psi_f^{(-)}(\mathbf{r}_2)$ is the distorted wave for the “slow” electron, $\psi_{nlm}(\mathbf{r}_3)$ is the hydrogenic final state of He^+ , and $\psi_i(\mathbf{r}_2, \mathbf{r}_3)$ is the initial-bound-state wave function for helium. The integration over the projectile electron is performed analytically using the Bethe integral, and the remaining integrations over the two atomic electrons are performed numerically. As a result, any ground-state helium wave function can be used, and calculations are presented here for two common descriptions.

An important issue concerns how to improve numerical calculations of ionization cross sections. The T matrix has two parts, the initial state and the final state and one possibility is to systematically try to improve the initial state without regard to the final state and the other possibility is to try to improve both the initial and final states in a symmetric way. There is strong evidence that it is important to treat both the initial and final states symmetrically. In the early 1970s, it was shown that large angle DCS for excitation of hydrogen and helium were wrong by orders of magnitude if distorted waves were used on one side and plane waves were used on the other side while good agreement with data was achieved if distorted waves were used for both sides. Jones and Madison [70] showed that a symmetrical treatment of the helium double-ionization problem (Pluvillage [71] initial and 3C final) gave good agreement for 17 of 20 sets of experimental measurements while no other calculation had come close to achieving agreement that good. Since ionization–excitation and double ionization are highly-correlated processes in which two bound electrons change their quantum state, it seemed worthwhile to examine the effects of using a Pluvillage wave function for the initial state. Although the logical final state to use with the Pluvillage wave function would be a 3C-type wave function with one bound electron, Foster *et al.* [72] showed that this type of wave function has problems when one of the electrons is bound and one is in the continuum and that it is better to use a distorted wave for this case. Nevertheless, it is of interest to examine the effect of

using the Pluvillage wave function for the initial state so we have used distorted waves for the final state and two different initial-state wave functions—a 20 term Hylleraas wave function [73] and a Pluvillage wave function. These two first-order perturbative models will be labeled PWB1-HY (Hylleraas) and PWB1-PL (Pluvillage).

C. Hybrid DWBA R -matrix approach

Another set of numerical calculations for the present work was performed using a hybrid distorted wave Born approximation (DWBA) + R -matrix (close-coupling) method. As mentioned above, the general idea is to treat the interaction of a “fast” electron with the target perturbatively, while the initial bound state and the e - He^+ half collision of a “slow” ejected electron and the residual ion is treated via a convergent R -matrix with pseudostates (close-coupling) expansion.

The method has already been very successful for asymmetric-energy-sharing conditions [17,19,45,47]. On the other hand, due to the fundamentally different treatment of the two final-state electrons, one would not expect it to be an optimal choice for symmetric-energy-sharing cases. Nevertheless, we decided to apply the DWBA R -matrix approach to these cases as well, and thereby assess the size of the problem that will need to be fixed in the future. Consequently, we performed DWB1-RMPS and DWB2-RMPS calculations, in which the projectile-target interaction was treated to first (DWB1) or second (DWB2) order. Details of the original formulation can be found in Bartschat and Burke [63], and the extensions needed to account for second-order effects, including channel coupling to convergence, and the calculation of angle-differential parameters are given in Refs. [21,19,74], respectively.

We note that several approximations are currently being made in order to simplify the evaluation of the second-order term. These include neglecting the real part of the Green’s function in the intermediate sum, using an average energy for the intermediate states similar to the closure approximation, and evaluating integrals only within the R -matrix sphere. Furthermore, exchange effects between the projectile and the target are neglected, as is the correlation due to the long-range Coulomb force between the two outgoing electrons in the final state. Some of these approximations were qualitatively supported by Chen and Madison [20], albeit in a simpler distorted-wave model for the ejected electron and the intermediate states being restricted to one electron occupying the $1s$ orbital of He. Although highly desirable and currently in progress, removing any of the above approximations in the complex framework of the R -matrix (close-coupling) approach is a major task. As will be seen below, however, even the current second-order model is far superior to any first-order treatment of the projectile-target interaction.

For the asymmetric-energy-sharing cases, the distortion potential for the projectile in both the initial- and final-state was chosen as the static potential of the $\text{He}(1s^2)$ ground state. In contrast, for the symmetric-energy-sharing cases the distortion potential in the final state was chosen as the ionic potential of the corresponding $\text{He}^+(n\ell)$ states. A

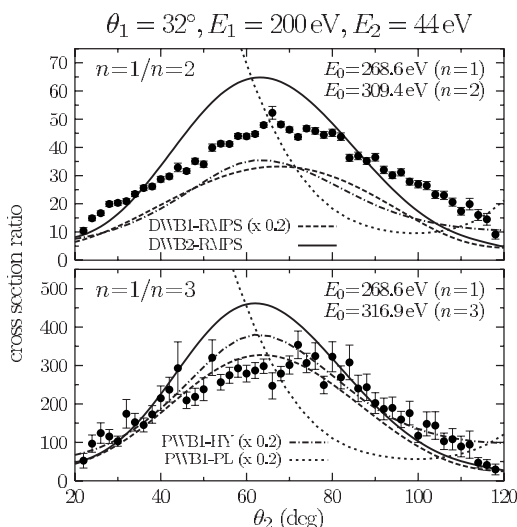


FIG. 2. TDCS for ionization of $\text{He}(1s^2)$ leading to $\text{He}^+(1s)$ divided by the corresponding TDCS for leaving the He^+ ion in the $n=2$ and $n=3$ states, respectively. The final-state electrons have average energies of 200 and 44 eV in all cases, while the primary energy E_0 was set to 268.6 eV for $n=1$, 309.4 eV for $n=2$, and 316.9 eV for $n=3$, respectively. The 200 eV electron is detected at $\theta_1=32^\circ$, while the detection angle θ_2 of the 44 eV electron is varied (see Fig. 1). The various theoretical models are described in the text. Note that all first-order results were multiplied by 0.2.

total of 23 states of He^+ were coupled to treat the $e\text{-He}^+$ collision problem for the ejected electron as well as the initial $\text{He}(1s^2)$ bound state. Of these, the lowest six were the physical $n=1,2,3$ states of He^+ , complemented by four pseudobound states (one each for $\ell=0-3$) and 13 pseudostates with energies above the ionization threshold of He^+ , thereby coupling to the double-ionization continuum of He . The bound-state energy obtained was $-2.902\,332\,0$ hartree, i.e., approximately 98% of the correlation energy was accounted for. Checks with smaller numbers of coupled states were performed to ensure that the results presented here are effectively converged with the number of states included in the close coupling plus correlation expansion. Finally, up to 90 partial waves for the projectile and components up to $\lambda=4$ in the multipole expansion of the projectile-target Coulomb interaction ensured converged results in these aspects as well.

IV. RESULTS AND DISCUSSION

A. First-order and second-order predictions

Experimental data for asymmetric-energy-sharing kinematics are shown in Fig. 2 and for symmetric scattering-geometry in Fig. 3, compared with predictions from various theoretical approaches described above. In both cases, data are presented by keeping the detection angle θ_1 of one electron fixed and varying the detection angle θ_2 of the second electron. Since the overall trend is the same for all detection angles between 24° and 56° , we select a detection angle of 32° for the present discussion. The complete set of experimental results is presented in the next subsection.

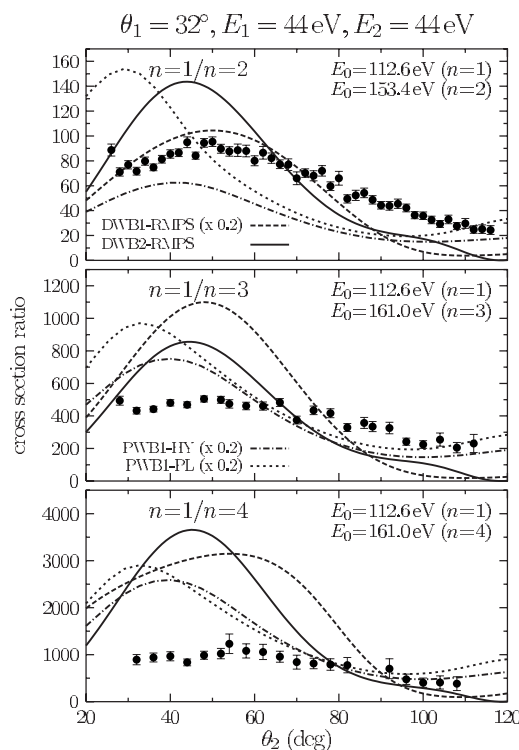


FIG. 3. TDCS for ionization of $\text{He}(1s^2)$ leading to $\text{He}^+(1s)$ divided by the corresponding TDCS for leaving the He^+ ion in the $n=2$ and $n=3$ states, respectively. The final-state electrons have average energies of 44 eV in all cases, while the primary energy E_0 was set to 112.6 eV for $n=1$, 153.4 eV for $n=2$, and 161.0 eV for $n=3,4$, respectively. One electron is detected at $\theta_1=32^\circ$, while the detection angle θ_2 of the other is varied (see Fig. 1). The various theoretical models are described in the text. Note that all first-order results were multiplied by 0.2.

As can be seen from the figures, the magnitude of the cross-section ratios increases rapidly with increasing value of the principal quantum number n of the residual He^+ state, thereby indicating the rapidly decreasing cross sections with increasing n of the residual ion state. Experiment shows excitation to the excited states accounting for only around 1% of the probability of transitions leading to a ground-state ion for the $n=2$ ion state, around 0.5% for the $n=3$ ion state, and about 0.1% for the $n=4$ ion state over the range of kinematics measured.

The first striking result seen in the figures is the complete failure of all models treating the projectile-target interaction only to first order. The ratios predicted by these models are about a factor of 5 (!) too large compared to experiment. Looking at the individual predictions revealed that the principal reason for the failure of the first-order models lies in their results for ionization plus simultaneous excitation, rather than in the cross sections for direct ionization. While accounting for second-order effects also changes the ratio results, these changes are generally in the range of 10–30% rather than a factor of 5. Interestingly, the predicted angular dependence of the cross-section ratio is quite satisfactory in the first-order models with either the Hylleraas or the RMPS ground state. This finding agrees with the patterns observed by Sakhelashvili *et al.* [45] and strongly supports the need

for either cross-normalized experimental data or, as in the present study, relative data for which the normalization factors cancel.

The first-order results provide some insight into the importance, or lack thereof, of accounting for particular effects that are often investigated in theoretical studies. To begin with, the good agreement between the PWB1-HY and DWB1-RMPS results suggests that neither channel coupling for the ejected electron (a distorted wave is used in the PWB1-HY model and a convergent RMPS expansion in DWB1-RMPS) nor distortion effects for the projectile (plane wave vs distorted wave) are the reason for the failure of the first-order model in the kinematical situation studied here. This is understandable, since the distortion for the projectile is known to be relatively unimportant for helium at our incident energies, and we carefully avoided resonance regimes for the ejected electrons.

Furthermore, using the Hylleraas initial state yields very similar results to those obtained with the RMPS ground state, which is effectively a multiconfiguration Hartree-Fock expansion. A surprising result, however, is the dramatic difference seen between the PWB1-HY and PWB1-PL results, especially for the asymmetric-energy-sharing case (see Fig. 2). For the case of 5.5 keV double ionization of helium ($e, 3e$) in a highly-asymmetric geometry, changing the initial state from HY to PL significantly improved agreement between experiment and theory, both in terms of magnitude and shape [70]. Here we see just the opposite and the PL results for small ejection angles and asymmetric collisions completely fail to reproduce the experiment. Of course, the importance of this result is not clear considering the fact that the first-order results are a factor of 5 too big.

The DWB2-RMPS results, on the other hand, describe the experimental results more accurately overall. In terms of magnitude, they are substantially closer to measurement, although the predicted angular dependence exhibits remaining discrepancies with the experimental data. As one might expect for a theory originally developed for asymmetric energy-sharing (the two electrons are not treated in the same way), the DWB2-RMPS results agree somewhat better with experiment for the asymmetric-energy-sharing case (Fig. 2) than for the symmetric situation (Fig. 3). Also not surprisingly, the biggest discrepancies between DWB2-RMPS and experiment occur for symmetric-energy-sharing and ionization—excitation to the $n=4$ states. This process only occurs about once in a thousand times relative to direct ionization, and the difficulty of accurately calculating such rare events is well known.

B. Summary of results

Figures 4 and 5 present an overview of all experimental results of the present study, in comparison with only the DWB2-RMPS predictions. Although first-order models may yield the correct angular dependence of the cross-section ratios, it is clear from the previous discussion that the calculated magnitude is generally wrong by a factor of about 5. Hence the dominant effect to explain the present experimental results is a second- (or higher-) order interaction between

the projectile and the target. As discussed in detail for $\theta_1 = 32^\circ$, the overall agreement between experiment and the DWB2-RMPS results is encouraging, although by no means perfect.

For the asymmetric-energy-sharing kinematics (Fig. 4), there is no clear trend suggesting a particular angular range or transition, for which the DWB2-RMPS theory works better than for others. For $\theta_1 \leq 40^\circ$, the angular dependence of the cross-section ratios seen in the experiment is generally flatter than that predicted theoretically, for both the $n=2$ and $n=3$ final ionic states. For larger angles, the angular dependence is well described, with a few magnitude problems remaining.

For the symmetric-energy-sharing kinematics (Fig. 5), there is still qualitative agreement between experiment and the DWB2-RMPS results, at least concerning the overall magnitude. However, there are several cases where the observed and the calculated angular dependence of the ratios differ substantially. For example, for $\theta_1 \geq 44^\circ$, the experimental ratios increase towards emission in the forward direction, while theory predicts a decrease.

Error bars on the experimental data points (indicated in the figures) were derived from statistical considerations only and represent how counting statistics affect the accuracy of derived cross-section ratios. Estimates for experimental systematic errors are provided below.

First, the finite nature of experimental angular and energy resolution modifies both the shape and magnitude of the angular distributions. The presented data include the intrinsic angular resolution of the toroidal analyzers themselves, $\approx \pm 1.5^\circ$ out of the scattering plane, and have been integrated over 4° bins in both θ_1 and θ_2 variables. Together these effects smooth out angular structure. The calculations presented in the figures have not been averaged in angle to account for this effect as it would have taken prohibitively long to perform the multiple calculations required. However, given the slowly varying character of the experimental distributions in both θ_1 and θ_2 relative to the 4° bin size, this effect could not by itself account for the extent of observed shape differences between theory and experiment. Second, the experimental data presented here comprise an energy integration over the energy-acceptance bands of the two analyzers (16 eV for the asymmetric experiment and 8 eV for the symmetric-energy-sharing case). Again, to avoid the prohibitively-long computational overheads, which would be required to perform an accurate integration of the calculations over the analyzer energy-acceptance-bands, the theoretical results presented here correspond to the average energies of the analyzer energy-acceptance-bands only. However, checks were performed to assess the effects of convolution by the experimental energy windows on the calculation and were estimated to modify the presented values by generally no more than 10%.

Drifts in the primary electron-beam current or target density with time were rendered essentially negligible by stepping through the incident-beam energies corresponding to excitation of the $n=1$, $n=2$, and $n=3$ states many times per hour. The issue of spatial variations in detector efficiency is a serious one inherent to all measurements employing multiparameter position-sensitive detection, however the beauty of

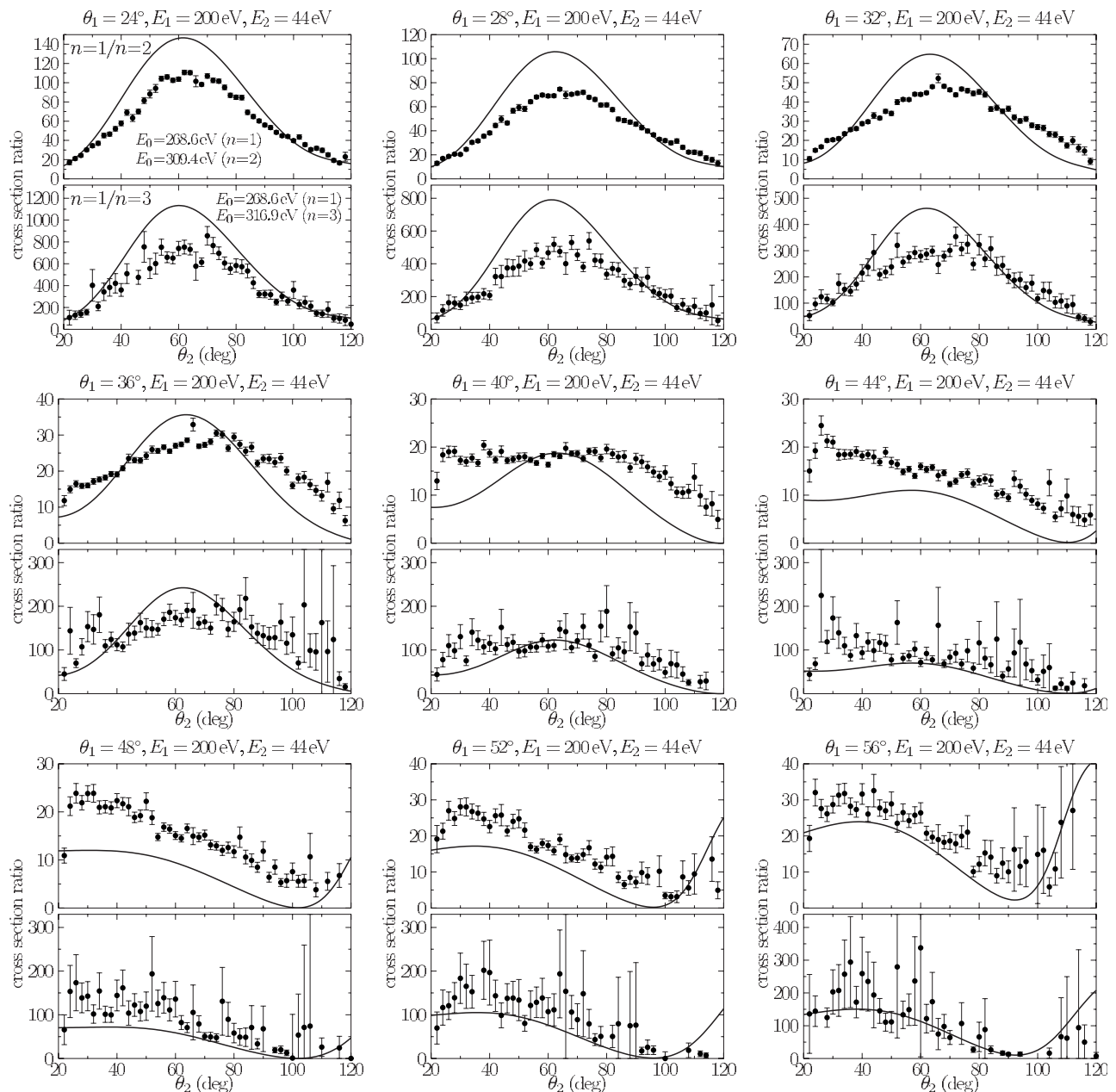


FIG. 4. TDCS for ionization of $\text{He}(1s^2)$ leading to $\text{He}^+(1s)$ divided by the corresponding TDCS for leaving the He^+ ion in the $n=2$ and $n=3$ states. The final-state electrons have average energies of 200 and 44 eV in all cases, while the primary energy E_0 was set to 268.6 eV for $n=1$, 309.4 eV for $n=2$, and 316.9 eV for $n=3$, respectively. The various panels are for the 200 eV electron being detected at angles $\theta_1 = 24^\circ - 56^\circ$, while the detection angle θ_2 of the 44 eV electron is varied. The solid line represents the predictions from the DWB2-RMPS model described in the text.

presenting results as a ratio is that while the two triple-differential cross sections comprising the ratio will be affected by such variations, their quotient, to an extremely good approximation, will not. (An exact cancellation of errors does not occur because differences between the energy distributions for scattered electrons corresponding to different n states means that their associated combinations of electron arrival positions at the two detectors will be slightly different).

The main source of systematic experimental error is estimated to be unaccounted-for variations in the density profile of the interaction volume resulting with changes in the

incident-beam energy as the respective ion states are stepped through. Only if the integral of the product of electron- and target-beam density distributions over space is a constant, count rates can be related to the $(e, 2e)$ cross sections. As described in Sec. II, to minimize such effects the beam optics was refocused at each value of incident energy to enable energy-dependent changes in the primary electron-beam current to be corrected for in software and to maintain, as closely as possible, an energy independence in the electron-beam profile at the interaction region. Because the electron-beam profile is very difficult to measure directly, the efficacy of the correction procedure is hard to assess. However, on

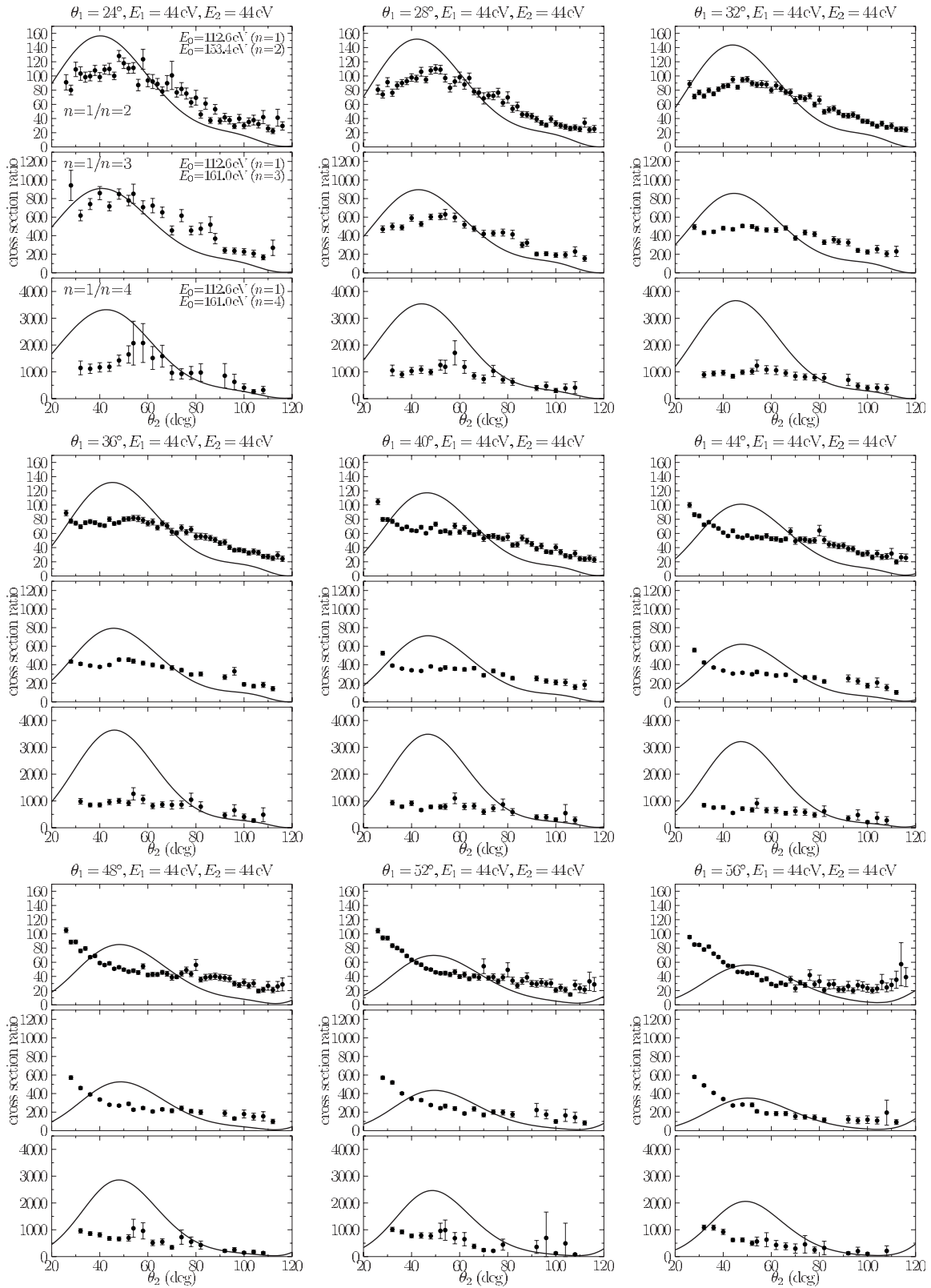


FIG. 5. TDCS for ionization of $\text{He}(1s^2)$ leading to $\text{He}^+(1s)$ divided by the corresponding TDCS for leaving the He^+ ion in the $n=2$, $n=3$, and $n=4$ states. Both outgoing electrons have an average energy of 44 eV for $n=1, 2, 3$ (42.7 eV for $n=4$), while the primary energy E_0 was chosen as 112.6 eV for $n=1$, 153.4 eV for $n=2$, and 161.0 eV for $n=3, 4$, respectively. Each panel is for one of the final-state electrons being detected at $\theta_1 = 24^\circ - 56^\circ$, while the detection angle θ_2 of the other electron is varied (see Fig. 1). The solid line represents the predictions from the DWB2-RMPS model described in the text.

the basis of electron-beam trajectory simulations, measurements of beam diameters at the interaction region using a movable Faraday cup and the expected target-gas profile for the driving pressures adopted, we estimate an upper limit of around $\pm 10\%$ in the uncertainty of the experimental cross-section ratios presented in this paper.

In conclusion, the small magnitude of statistical and possible systematic errors is clearly insufficient to explain disparities between experiment and all theories.

V. CONCLUSIONS

We have presented an extensive set of cross-section ratios for electron-impact ionization of helium, comparing direct ionization with the He^+ ion left in its ground state to ionization–excitation leading to He^+ in the excited $n = 2, 3, 4$ states. In addition to eliminating the need for (cross) normalization, careful attention was paid to reduce possible effects due to finite energy and angular resolution, which often made previous comparisons between experiment and theory difficult.

For all the kinematical cases studied in the present work, with incident electron energies of a few 100 eV, scattered or ejected electron energies of 44 and 200 eV, and electron detection angles between 24° and 120° , it was found that while first-order theories in the projectile-target interaction are able

to accurately predict the shape, they are unable to predict the correct magnitude of the ratio. Although second-order and higher-order effects are known to also be important for direct ionization leaving He^+ in the ground state, the principal failure of the first-order models lies in predicting generally far too small (by about a factor of 5) cross sections for the simultaneous-ionization–excitation process.

The hybrid DWB2-RMPS method, on the other hand, qualitatively reproduced the present experimental results. However, there is still much room for improving the quantitative agreement between experiment and theory. This might be achieved, for example, by removing several approximations made in the evaluation of the second-order term and incorporating the long-range correlation between the two outgoing electrons. Work in this direction is currently in progress, but it is far beyond the scope of the present study. We hope that the present extensive set of experimental data will stimulate further theoretical work on this challenging four-body Coulomb problem.

ACKNOWLEDGMENTS

We gratefully acknowledge the assistance of the Australian Research Council under Grant No. DP0452553 (S.B. and J.L.) and the United States National Science Foundation under Grants No. PHY-0244470 (K.B., X.G., and D.W.) and No. PHY-0070872 (A.L.H. and D.H.M.).

-
- [1] R. Dörner, V. Mergel, O. Jagutzki, L. Spielberger, J. Ullrich, R. Moshhammer, and H. Schmidt-Böcking, *Phys. Rep.* **330**, 95 (2000).
 - [2] J. Ullrich, R. Moshhammer, A. Dorn, R. Dörner, L. Ph. H. Schmidt, and H. Schmidt-Böcking, *Rep. Prog. Phys.* **66**, 1463 (2003).
 - [3] T. Weber *et al.*, *Nature (London)* **431**, 437 (2004).
 - [4] J. Lower *et al.*, in *Electron and Photon Impact Ionization and Related Topics*, edited by L. U. Ancarani, IOP Conf. Series 172, 31 (2002).
 - [5] A. Duguet, A. Lahmam-Bennani, M. Lecas, and B. El Marji, *Rev. Sci. Instrum.* **69**, 3524 (1998).
 - [6] T. J. Reddish, G. Richmond, G. W. Bagley, J. P. Whightman, and S. Cvejanović, *Rev. Sci. Instrum.* **68**, 2685 (1997).
 - [7] M. Takahashi, T. Saito, M. Matsuo, and Y. Udagawa, *Rev. Sci. Instrum.* **73**, 2242 (2002).
 - [8] R. W. van Boeyen and J. F. Williams, *Rev. Sci. Instrum.* **76**, 063303 (2005).
 - [9] T. N. Rescigno, M. Baertschy, W. A. Isaacs, and C. W. McCurdy, *Science* **286**, 2474 (1999).
 - [10] J. Colgan, M. S. Pindzola, F. J. Robicheaux, D. C. Griffin, and M. Baertschy, *Phys. Rev. A* **65**, 042721 (2002).
 - [11] I. Bray, D. V. Fursa, A. Kheifets, and A. T. Stelbovics, *J. Phys. B* **35**, R117 (2002).
 - [12] K. Bartschat and I. Bray, *J. Phys. B* **29**, L577 (1996).
 - [13] I. Bray, *Phys. Rev. Lett.* **89**, 273201 (2002).
 - [14] A. T. Stelbovics, I. Bray, D. V. Fursa, and K. Bartschat, *Phys. Rev. A* **71**, 052716 (2005).
 - [15] M. Dürr, C. Dimopoulou, B. Najjari, A. Dorn, and J. Ullrich, *Phys. Rev. Lett.* **96**, 243202 (2006).
 - [16] M. Dürr, C. Dimopoulou, A. Dorn, B. Najjari, I. Bray, D. V. Fursa, Zhangjin Chen, D. H. Madison, K. Bartschat, and J. Ullrich, *J. Phys. B* **39**, 4097 (2006).
 - [17] S. Bellm, J. Lower, and K. Bartschat, *Phys. Rev. Lett.* **96**, 223201 (2006).
 - [18] D. H. Madison, R. V. Calhoun, and W. N. Shelton, *Phys. Rev. A* **16**, 552 (1977).
 - [19] Y. Fang and K. Bartschat, *J. Phys. B* **34**, L19 (2001).
 - [20] Z. Chen and D. H. Madison, *J. Phys. B* **38**, 4195 (2005).
 - [21] R. H. G. Reid, K. Bartschat, and A. Raeker, *J. Phys. B* **31**, 563 (1998); R. H. G. Reid, K. Bartschat, and A. Raeker, *J. Phys. B*, *ibid.*, **33**, 5261 (2000).
 - [22] Z. Chen, D. H. Madison, C. T. Whelan, and H. R. Walters, *J. Phys. B* **37**, 981 (2002).
 - [23] Z. Chen, S. Zhang, Q. Shi, J. Chen, and K. Xu, *J. Phys. B* **30**, 4963 (1997).
 - [24] M. Brauner, J. S. Briggs, and H. Klar, *J. Phys. B* **22**, 2265 (1989).
 - [25] J. Berakdar and J. S. Briggs, *Phys. Rev. Lett.* **72**, 3799 (1994).
 - [26] A. Prideaux and D. H. Madison, *Phys. Rev. A* **67**, 052710 (2003).
 - [27] S. Jones, D. H. Madison, A. Franz, and P. L. Altick, *Phys. Rev. A* **48**, R22 (1993).
 - [28] J. Gao, D. H. Madison, and J. L. Peacher, *J. Chem. Phys.* **123**, 204314 (2005).
 - [29] J. Gao, D. H. Madison, and J. L. Peacher, *J. Phys. B* **39**, 1275

- (2006).
- [30] R. Panajotovic, J. Lower, E. Weigold, A. Prideaux, and D. H. Madison, *Phys. Rev. A* **73**, 052701 (2006).
- [31] M. Schulz, R. Moshhammer, D. Fischer, H. Kollmus, D. H. Madison, S. Jones, and J. Ullrich, *Nature (London)* **422**, 48 (2003).
- [32] M. Foster, J. L. Peacher, M. Schulz, D. H. Madison, Z. Chen, and H. R. J. Walters, *Phys. Rev. Lett.* **97**, 093202-1 (2006).
- [33] A. S. Kheifets, I. Bray, and K. Bartschat, *J. Phys. B* **32**, L433 (1999).
- [34] I. E. McCarthy, A. Ugbade, E. Weigold, and P. J. O. Teubner, *Phys. Rev. Lett.* **33**, 459 (1974).
- [35] A. D. Smith, M. A. Coplan, D. J. Chornay, J. H. Moore, J. A. Tossel, J. Mroczek, V. H. Smith, Jr., and N. S. Chant, *J. Phys. B* **19**, 969 (1986).
- [36] J. P. D. Cook, I. E. McCarthy, A. T. Stelbovics, and E. Weigold, *J. Phys. B* **17**, 2339 (1984).
- [37] G. Stefani, L. Avaldi, and R. Camilloni, *J. Phys. B* **23**, L227 (1990).
- [38] C. Dupré, A. Lahmam-Bennani, A. Duguet, F. Mota-Furtado, P. F. O'Mahony, and C. Dal Cappello, *J. Phys. B* **25**, 259 (1992).
- [39] L. Avaldi, R. Camilloni, R. Multari, G. Stefani, J. Langlois, O. Robaux, R. J. Tweed, and G. N. Vien, *J. Phys. B* **31**, 2981 (1998).
- [40] B. Rouvellou, S. Rioual, A. Pochat, R. J. Tweed, J. Langlois, G. N. Vien, and O. Robaux, *J. Phys. B* **33**, L599 (2000).
- [41] P. J. Marchalant, C. T. Whelan, and H. R. J. Walters, *J. Phys. B* **31**, 1141 (1998).
- [42] M. Dogan and A. Crowe, *J. Phys. B* **33**, L461 (2000).
- [43] N. Watanabe, Y. Khajuria, M. Takahashi, Y. Udagawa, P. S. Vinitsky, Yu. V. Popov, O. Chuluunbaatar, and K. A. Kouzakov, *Phys. Rev. A* **72**, 032705 (2005).
- [44] X. G. Ren, C. G. Ning, J. K. Deng, G. L. Su, S. F. Zhang, Y. R. Huang, and G. Q. Li, *Phys. Rev. A* **72**, 042718 (2005).
- [45] G. Sakhelashvili, A. Dorn, C. Höhr, J. Ullrich, A. S. Kheifets, J. Lower, and K. Bartschat, *Phys. Rev. Lett.* **95**, 033201 (2005).
- [46] A. J. Murray and F. H. Read, *J. Phys. B* **25**, L579 (1992).
- [47] Y. Fang and K. Bartschat, *Phys. Rev. A* **64**, 020701(R) (2001).
- [48] J. Lower, R. Panajotović, and E. Weigold, *Phys. Scr.* **T110**, 216 (2004).
- [49] T. Nakanishi, H. Aoyagi, H. Horinaka, Y. Kamiya, T. Kato, S. Nakamura, T. Saka, and M. Tsubata, *Phys. Lett. A* **158**, 345 (1991).
- [50] M. Dogan, A. Crowe, K. Bartschat, and P. J. Marchalant, *J. Phys. B* **31**, 1611 (1998).
- [51] H. Merabet, R. Bruch, S. Fölling, K. Bartschat, and A. L. Godunov, *J. Phys. B* **36**, 3383 (2003).
- [52] O. K. Vorov and K. Bartschat, *J. Phys. B* **38**, 1189 (2005).
- [53] M. S. Pindzola, F. J. Robicheaux, J. P. Colgan, M. C. Witthoef, and J. A. Ludlow, *Phys. Rev. A* **70**, 032705 (2004).
- [54] E. T. Hudson, K. Bartschat, M. P. Scott, P. G. Burke, and V. M. Burke, *J. Phys. B* **29**, 5513 (1996).
- [55] K. Bartschat, *Comput. Phys. Commun.* **114**, 168 (1998).
- [56] I. Bray, D. V. Fursa, A. S. Kheifets, and A. T. Stelbovics, *J. Phys. B* **35**, R117 (2002).
- [57] D. V. Fursa and I. Bray, *J. Phys. B* **30**, 757 (1997).
- [58] C. W. McCurdy, D. A. Horner, and T. N. Rescigno, *Phys. Rev. A* **65**, 042714 (2002).
- [59] M. S. Pindzola (private communication).
- [60] A. Franz and P. L. Altick, *J. Phys. B* **25**, L257 (1992).
- [61] A. Franz and P. L. Altick, *J. Phys. B* **28**, 4639 (1995).
- [62] H. Jakubowicz and D. L. Moores, *J. Phys. B* **14**, 3733 (1981).
- [63] K. Bartschat and P. G. Burke, *J. Phys. B* **20**, 3191 (1987).
- [64] M. R. H. Rudge, *J. Phys. B* **21**, 1887 (1988).
- [65] A. Raeker, K. Bartschat, and R. H. G. Reid, *J. Phys. B* **27**, 3129 (1994).
- [66] K. Bartschat and A. N. Grum-Grzhimailo (unpublished), quoted in Ref. [51].
- [67] A. S. Kheifets, I. Bray, and K. Bartschat, *J. Phys. B* **32**, L433 (1999).
- [68] P. J. Marchalant, J. Rasch, C. T. Whelan, D. H. Madison, and H. R. J. Walters, *J. Phys. B* **32**, L705 (1999).
- [69] A. S. Kheifets, *Phys. Rev. A* **69**, 032712 (2004).
- [70] S. Jones and D. H. Madison, *Phys. Rev. Lett.* **91**, 073201 (2004).
- [71] P. Pluvinage, *Ann. Phys. (N.Y.)* **5**, 145 (1950).
- [72] M. Foster, J. L. Peacher, M. Schulz, A. Hasan, and D. H. Madison, *Phys. Rev. A* **72**, 062708 (2005).
- [73] J. F. Hart and G. Herzberg, *Phys. Rev.* **106**, 79 (1957).
- [74] K. Bartschat and A. N. Grum-Grzhimailo, *J. Phys. B* **35**, 5035 (2002).